

# Modulation of a quantized vortex street with a vibrating obstacle

Hiroki Saito, Kenta Tazaki, and Tomohiko Aoi

*Department of Engineering Science, University of Electro-Communications, Tokyo 182-8585, Japan*

(Dated: June 10, 2022)

Dynamics of a superfluid flow past an obstacle are investigated by solving the Gross–Pitaevskii equation numerically. For appropriate velocity and size of the obstacle, quantized vortices are periodically generated in the wake, which form a Bénard–von Kármán vortex street. It is found that vibration of an obstacle modulates the vortex street, breaking a symmetry. The parameter dependence of the modulation dynamics of vortices is investigated.

## I. INTRODUCTION

When a cylindrical obstacle is moved in a viscous fluid with an appropriate velocity, vortices are periodically shed in the wake, forming a long-lived vortex street. This phenomenon was experimentally studied by Bénard [1] and the stability of the vortex street was theoretically investigated by von Kármán [2, 3] in the early twentieth century. The Bénard–von Kármán (BvK) vortex streets are observed in a wide scale throughout nature: from a bathtub to the atmosphere on a planet.

The behaviors of a classical viscous fluid past an obstacle are characterized by the Reynolds number,  $Re$ , which is proportional to the size and velocity of the obstacle and inversely proportional to the kinematic viscosity. A stationary flow is stable for a small value of  $Re$ . When  $Re$  exceeds a critical value, an instability sets in and vortices are shed in the wake, forming the BvK vortex street. For a very large value of  $Re$ , the flow behind the obstacle becomes turbulence. Thus, in a classical fluid, the viscosity, which is included in  $Re$ , plays an important role for the vortex street generation.

In contrast, Sasaki *et al.* [4] theoretically predicted that a BvK-like vortex street can also be generated in superfluids, in which viscosity is absent and a vortex is quantized. This prediction has been made by numerical simulations of the Gross–Pitaevskii (GP) equation, and therefore the phenomenon can be observed in the systems that are described by the GP equation, such as an atomic-gas Bose–Einstein condensate [5] and an exciton–polariton superfluid in a semiconductor microcavity [6, 7]. Theoretical studies on the dynamics of superfluids behind a moving obstacle have been performed by many researchers [8–14].

In the present paper, we extend the study in Ref. [4] to the case in which an obstacle moves along a sinusoidal trajectory. In classical fluids, it has been found that such a vibrating cylinder in a flow generates various types of vortex streets, in which the symmetry between two rows of vortices is broken [15, 16]. We will show that such symmetry breaking occurs also for the BvK vortex street in a superfluid. When the oscillation frequency and the vortex shedding frequency satisfy some resonance condition, the vortex street is shown to be modulated and become asymmetric.

This paper is organized as follows. Section II formu-

lates the problem. Section III A briefly reviews the case of straight motion of an obstacle [4] and Sec. III B shows the case of sinusoidal motion, which is the main result of the paper. Section IV gives conclusions to the study.

## II. FORMULATION OF THE PROBLEM

We consider the two-dimensional GP equation given by

$$i\hbar\frac{\partial\psi}{\partial t} = -\frac{\hbar^2}{2m}\nabla^2\psi + V\psi + g|\psi|^2\psi, \quad (1)$$

where  $\psi(x, y, t)$  is the macroscopic wave function,  $V(x, y, t)$  is an obstacle potential, and  $g$  is an interaction coefficient. The obstacle potential is assumed to have a Gaussian shape as

$$V(\mathbf{r}, t) = V_0 \exp\{-[\mathbf{r} - \mathbf{r}_{\text{pot}}(t)]^2/d^2\}, \quad (2)$$

where  $V_0$  is the peak intensity,  $\mathbf{r}_{\text{pot}}(t)$  is the position of the center, and  $d$  is the  $1/e$  width. For an atomic Bose–Einstein condensate, such a potential can be produced by a blue-detuned ( $V_0 > 0$ ) or red-detuned ( $V_0 < 0$ ) Gaussian laser beam. In the present study, we consider the case of  $V_0 > 0$ . The vortex generation dynamics for  $V_0 < 0$  has been studied in Ref. [18]. The potential is moved sinusoidally as

$$\mathbf{r}_{\text{pot}}(t) = -vt\hat{\mathbf{x}} + a\sin(\omega t)\hat{\mathbf{y}}, \quad (3)$$

where  $\hat{\mathbf{x}}$  and  $\hat{\mathbf{y}}$  are the unit vectors,  $v > 0$  is the velocity in the  $-x$  direction, and  $a$  and  $\omega$  are the amplitude and frequency of the oscillation.

We numerically solve Eq. (1) using the pseudospectral method [17]. The initial state is the ground state of Eq. (1) with the initial position of the Gaussian potential, which is obtained by the imaginary-time propagation method. The norm of the wave function,  $\int |\psi|^2 d\mathbf{r}$ , is chosen such that the density  $n_0$  far from the obstacle potential becomes a desired value. To break the exact numerical symmetry, small white noise is added to the initial state. We take a large enough space and the boundary condition does not affect the result.

The characteristic length scale of the system is the healing length defined by  $\xi = \hbar/(mgn_0)^{1/2}$ . The sound velocity for the uniform density  $n_0$  is  $v_s = (gn_0/m)^{1/2}$ .

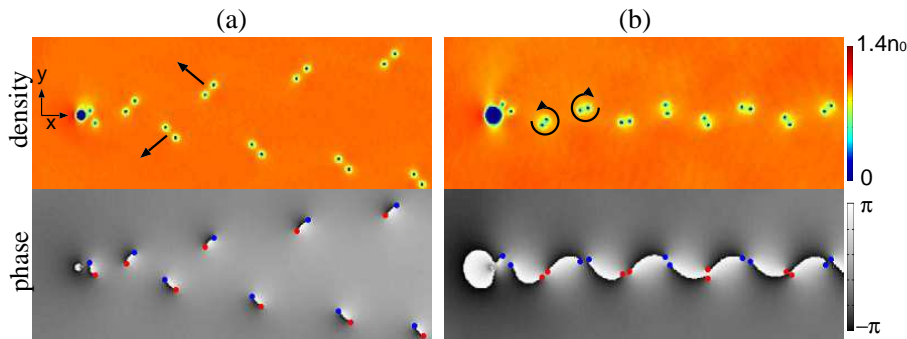


FIG. 1: Snapshots of the density ( $|\psi|^2$ ) and phase ( $\arg \psi$ ) profiles for the straight motion of the obstacle,  $a = 0$ . (a)  $v = 0.48v_s$ ,  $d = 1.26\xi$ , and  $V_0 = 100\mu$ . (b)  $v = 0.44v_s$ ,  $d = 2.24\xi$ , and  $V_0 = 100\mu$ . The arrows in (a) indicate directions of propagation of vortex dipoles. The arrows in (b) indicate directions of rotation of corotating vortex clusters. The blue and red dots in the phase profiles indicate vortices with clockwise and counterclockwise circulations, respectively. The field of view is  $250\xi \times 95\xi$ . See the movie [19] showing the dynamics in (a) and (b).

The characteristic time scale and energy are defined as  $\tau = \hbar/(gn_0)$  and  $\mu = gn_0$ , respectively. For a typical experimental system of an atomic Bose–Einstein condensate,  $\xi \sim 0.1 \mu\text{m}$ ,  $v_s \sim 1 \text{ mm/s}$ , and  $\tau \sim 0.1 \text{ ms}$ . For an exciton–polariton superfluid in a semiconductor microcavity,  $\xi \sim 1 \mu\text{m}$ ,  $v_s \sim 10^6 \text{ m/s}$ , and  $\tau \sim 1 \text{ ps}$  [7].

The GP equation in Eq. (1) has a scaling property. Normalizing the length, time, and density by  $\xi$ ,  $\tau$ , and  $n_0$ , respectively, we can eliminate the interaction coefficient  $g$  from the equation as

$$i\frac{\partial\tilde{\psi}}{\partial\tilde{t}} = -\frac{1}{2}\tilde{\nabla}^2\tilde{\psi} + \tilde{V}\tilde{\psi} + |\tilde{\psi}|^2\tilde{\psi}, \quad (4)$$

where tildes are put to the normalized quantities. The independent parameters are therefore  $V_0$ ,  $d$ ,  $v$ ,  $a$ , and  $\omega$ .

---

First, we consider the case of  $a = 0$  in Eq. (3), i.e., the potential moves straight in the  $-x$  direction. It has been known that quantized vortex–antivortex pairs, which we call vortex dipoles, are released behind an obstacle above a critical velocity [8]. For appropriate values of  $v$  and  $d$ , quantized vortices in the wake form two kinds of typical patterns [4], as shown in Fig. 1. In Fig. 1(a), periodically released vortex dipoles incline alternately, breaking the symmetry with respect to the  $x$  axis. Since vortex dipoles propagate in the directions as indicated by the arrows in Fig. 1(a), the inclined vortex dipoles propagate obliquely, and the vortex pattern spreads in the downstream.

Figure 1(b) shows an interesting vortex pattern, which was first reported in Ref. [4]. The building block of the vortex pattern is not a vortex dipole but a pair of corotating vortices with the same circulation, which we call a “vortex cluster”. The vortex clusters with opposite circulations are released alternately, which form two rows in the wake. This vortex shedding dynamics

When  $V_0$  is much larger than the chemical potential  $\mu$ , the Gaussian potential in Eq. (2) is almost equivalent to a circular hard-wall potential with an effective radius  $R$ , given by

$$V_0 e^{-R^2/d^2} \simeq \mu. \quad (5)$$

The height  $V_0$  and  $1/e$  width  $d$  of the potential are thus not independent parameters for  $V_0 \gg \mu$ .

### III. NUMERICAL RESULTS

#### A. Straight motion of an obstacle

---

and resultant vortex pattern are similar to those in the BvK vortex street in classical fluids, in that clockwise and counter clockwise vortices are shed alternately and two rows of vortices are aligned linearly. As shown by von Kármán [2, 3], the vortex pattern as generated in Fig. 1(b) is very stable and has a long lifetime.

From the movies [19] showing the dynamics in Fig. 1, it seems that two different instabilities are responsible for the vortex pattern formations. The first one is the instability that inclines the vortex dipoles in Fig. 1(a). At the first stage, the vortex dipoles have the symmetry with respect to the  $x$  axis, and after some time the inclination of the vortex dipoles starts. The second one is the instability that causes a transition from the vortex dipole generation to the BvK vortex street generation. In the movie corresponding to Fig. 1(b), we can see that the former changes to the latter dynamically.

For the velocity  $v$  slower than the critical velocity of vortex generation, the flow pattern is a stationary lam-

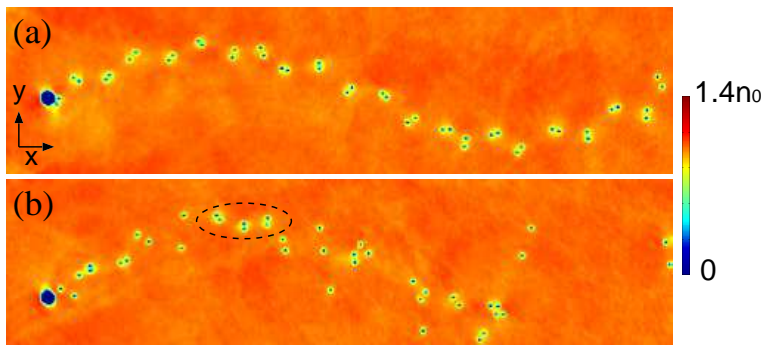


FIG. 2: Snapshots of the density profiles for the sinusoidal motion of the obstacle. (a)  $v = 0.43v_s$ ,  $a = 32\xi$ , and  $\omega = 0.006\tau^{-1}$ . (b)  $v = 0.41v_s$ ,  $a = 32\xi$ , and  $\omega = 0.008\tau^{-1}$ . Other parameters are the same as those in Fig. 1(b). The field of view is  $500\xi \times 125\xi$ .

inar flow. For a very large velocity, the flow pattern becomes irregular or a Cherenkov-like pattern [20, 21]. The periodic vortex shedding as shown in Fig. 1 is restricted between these two parameter regions. (The detailed parameter diagram is obtained in Ref. [4].) The vortex dipole generation as in Fig. 1(a) tends to occur for a smaller obstacle, and the BvK-like vortex street tends to appear for a larger obstacle. For an intermediate size of an obstacle, the former (latter) occurs for a slower (faster) velocity, where the vortex dipole generation changes to the BvK-like vortex street with an

increase in the velocity.

### B. Sinusoidal motion of an obstacle

We next consider the case of sinusoidal trajectories of the obstacle potential ( $a \neq 0$  in Eq. (3)), and investigate how the BvK-like vortex street is affected by the sinusoidal motion. Since the parameter region for the BvK-like vortex street to emerge is narrow [4], we restrict the parameters  $V_0$ ,  $d$ , and  $v$  to that region, and study the  $a$  and  $\omega$  dependence of the vortex shedding dynamics.

First, we examine the low frequency limit, in which  $\omega$  is much smaller than the vortex shedding frequency and the wavelength of the sinusoidal trajectory is much larger than the distance between vortex clusters. The result is shown in Fig. 2(a). The BvK-like vortex street is shed along the smoothly curved trajectory. For sinusoidal motion given in Eq. (3), the minimum and maximum velocities are  $v_{\min} = v$  and  $v_{\max} = (v^2 + a^2\omega^2)^{1/2}$  and the

root-mean-square velocity is  $\bar{v} = (v^2 + a^2\omega^2/2)^{1/2}$ . For the parameters in Fig. 2(a),  $v_{\min}$  and  $v_{\max}$  fall into the parameter region of the BvK-like street. For a larger value of  $a\omega$ ,  $v_{\min}$ ,  $v_{\max}$ , or both go out of the parameter region of the BvK-like street even when  $\bar{v}$  falls into that region. Figure 2(b) shows such a case. The vortex patterns are disturbed, although the BvK-like pattern is partly observed (dashed circle in Fig. 2(b)).

Figure 3 shows the case of a larger frequency  $\omega = 0.1\tau^{-1}$ , in which the amplitude  $a$  is much smaller than that in Fig. 2. The frequency  $\omega = 0.1\tau^{-1}$  is about twice the shedding frequency of the vortex clusters. For a small amplitude, in Fig. 3(a), the vortex pattern is similar to the BvK-like vortex street for straight motion in Fig. 1(b). As  $a$  is increased, the symmetry between the two rows of the vortex clusters is spontaneously broken. In Fig. 3(b), one can see that the vortex clusters in the upper row is larger than those in the lower row. In Fig. 3(c), the symmetry breaking is significant, where the vortex clusters in the upper row disintegrate in the downstream. Whether the vortex clusters in the upper row or lower row become large depends on the initial condition

that breaks the symmetry, since Eq. (1) has the symmetry with respect to  $y \rightarrow -y$ . In fact, the behaviors of the upper and lower rows can be exchanged by changing the initial condition (the initial phase of the oscillation in Eq. (3) and added initial noises). The roles of the upper and lower rows can be exchanged during the dynamics. In the movie [19] corresponding to Fig. 3(b), we can see that the vortex clusters in the upper row is first enlarged and then the lower row takes over. For a larger amplitude  $a$ , the vortex pattern is disturbed, as shown in Fig. 3(d). Thus, the degree of the symmetry breaking of the BvK-like vortex street increases with  $a$ , until the periodicity is disturbed for  $a \gtrsim \xi$ . It should be noted that the appropriate value of  $a$  for the symmetry breaking phenomenon

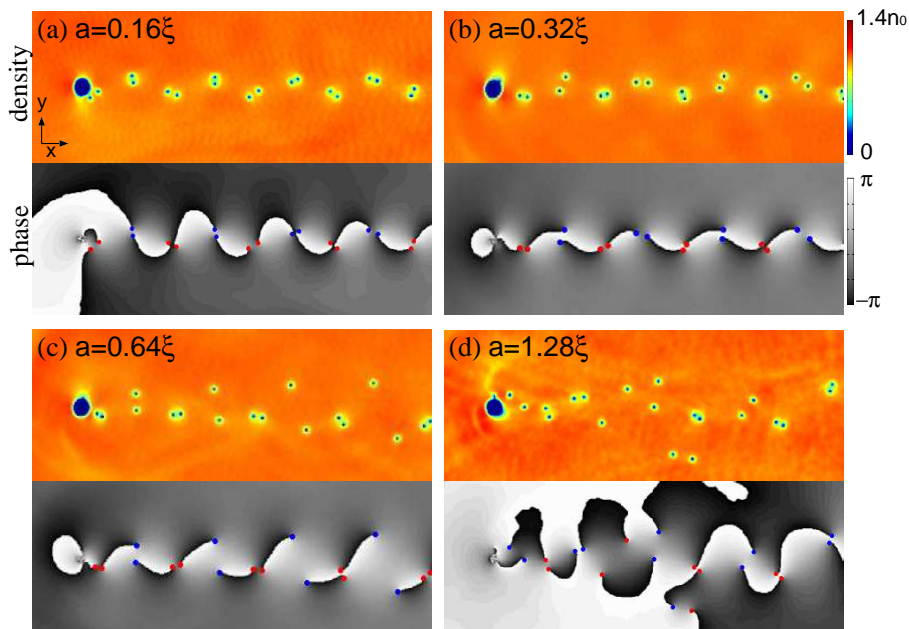


FIG. 3: Snapshots of the density ( $|\psi|^2$ ) and phase ( $\arg \psi$ ) profiles for the sinusoidal motion of the obstacle. The oscillation frequency is  $\omega = 0.1\tau^{-1}$  and the amplitude is (a)  $a = 0.16\xi$ , (b)  $a = 0.32\xi$ , (c)  $a = 0.64\xi$ , and (d)  $a = 1.28\xi$ . Other parameters are the same as those in Fig. 1(b). The blue and red dots in the phase profiles indicate vortices with clockwise and counterclockwise circulations, respectively. The field of view is  $250\xi \times 95\xi$ . See the movie [19] showing the dynamics in (b) and (c).

is  $a \sim \xi$ , i.e., the amplitude is comparable to the size of a vortex. The sinusoidal motion has a significant influence on the vortex shedding dynamics, even when the

amplitude is much smaller than the size of the obstacle potential.

Figure 4 shows the  $\omega$  dependence of the vortex dynamics, where the amplitude  $a$  is the same as that in Fig. 3(c). The frequency  $\omega$  in Fig. 4(c) is the same as that in Fig. 3, and therefore the parameters in Fig. 4(c) and Fig. 3(c) are identical. As  $\omega$  is decreased, the enlargement of the vortex clusters becomes intermittent, that is, the vortex shedding as in Fig. 4(c) and that in Fig. 1(b) are interchanged intermittently. At  $\omega = 0.08\tau^{-1}$ , an interesting resonance emerges as shown in Fig. 4(b), where every third vortex cluster is enlarged. When  $\omega$  is further decreased, the enlargement of the vortex clusters occurs not only in the one row but also in both rows successively, which is however intermittent, as shown in Fig. 4(a). For  $\omega \lesssim 0.05\tau^{-1}$ , the enlargement of the vortex clusters ceases and there seems to be no significant effect of the sinusoidal motion on the BvK-like vortex street (data not shown), that is, the vortex pattern is similar to that in Fig. 1(b).

As  $\omega$  is increased from  $0.1\tau^{-1}$ , the enlargement of the vortex clusters becomes intermittent, as shown in Fig. 4(d), which is similar to the vortex pattern in Fig. 4(a). Around  $\omega = 0.15\tau^{-1}$ , the vortex pattern

changes drastically, as shown in Fig. 4(e), where neither vortex dipoles nor vortex clusters are formed, and the periodically released vortex are apart from each other. This may be regarded as that the enlargement of vortex clusters, as shown in Figs. 4(a) and 4(d), occurs successively in both rows. For a larger value of  $\omega$ , the enlargement of vortex clusters becomes intermittent again, in a manner similar to Figs. 4(a) and 4(d). The enlargement of vortex clusters ceases and the BvK-like vortex street is generated for  $\omega \gtrsim 0.25\tau^{-1}$  (data not shown). For  $\omega \simeq 0.18\tau^{-1}$ , extra vortex dipoles are created during the vortex street generation, as indicated by the arrow in Fig. 4(f), which may be due to the disturbances by the fast oscillation of the obstacle. For  $\omega \gtrsim 0.25\tau^{-1}$ , the fast oscillating potential is effectively averaged in time and the disturbances are decreased. Thus, when the oscillation frequency of the obstacle is much larger or smaller than the vortex shedding frequency, the vortex pattern is not much affected, and when the oscillation frequency  $\omega$  is comparable to the vortex shedding frequency, the vortex pattern depends on  $\omega$  in a complicated manner. There may be other types of resonance dynamics, which

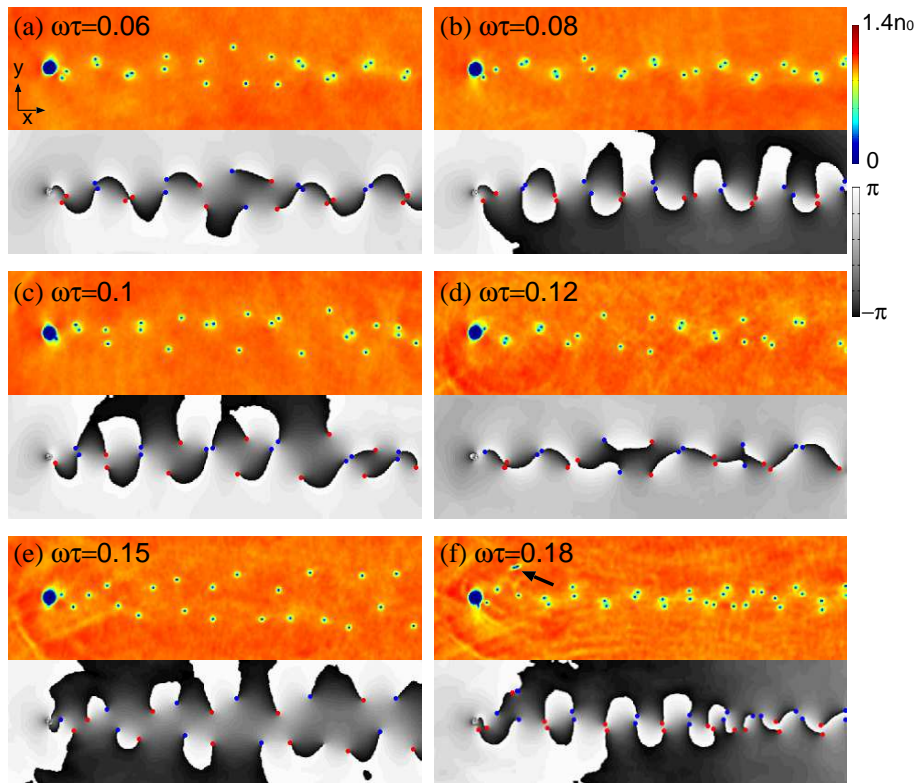


FIG. 4: Snapshots of the density ( $|\psi|^2$ ) and phase ( $\arg \psi$ ) profiles for the sinusoidal motion of the obstacle. The oscillation amplitude is  $a = 0.64\xi$  and the frequency is (a)  $\omega = 0.06\tau^{-1}$ , (b)  $\omega = 0.08\tau^{-1}$ , (c)  $\omega = 0.1\tau^{-1}$ , (d)  $\omega = 0.12\tau^{-1}$ , (e)  $\omega = 0.15\tau^{-1}$ , and (f)  $\omega = 0.18\tau^{-1}$ . Other parameters are the same as those in Fig. 1(b). The blue and red dots in the phase profiles indicate vortices with clockwise and counterclockwise circulations, respectively. The field of view is  $315\xi \times 95\xi$ .

however need fine tuning of the oscillation frequency.

Comparing the movies [19] of Figs. 1(b) and 3(b), we find that the BvK-like vortex street emerges faster in Fig. 3(b) than in Fig. 1(b), i.e., the vibration of the obstacle seems to enhance the emergence of the BvK-like vortex street. Figure 5 shows the dynamics of the early stage, where the obstacle starts to move at  $t = 0$ . For the straight motion of the obstacle (Fig. 5(a)), a vortex dipoles are first generated ( $t = 10\tau$ ) and the subsequent vortex dipoles are inclined. For the sinusoidal motion of the obstacle (Fig. 5(b)), the sixth and seventh released vortices form a tight vortex cluster (dashed circle in Fig. 5(b)), which is followed by the BvK-like vortex street with tight vortex clusters.

#### IV. CONCLUSIONS

We have investigated the dynamics of quantized vortex shedding from an obstacle moving in a superfluid, in which the obstacle traces a sinusoidal trajectory. As in the case of the straight motion of an obstacle, quantized vortex-antivortex pairs are released when the velocity exceeds some critical velocity, and for appropriate parameters, a BvK-like vortex street emerges in the wake. In

contrast to the case of the straight motion, the symmetry between the two rows of the BvK street is broken; the size of the corotating vortex clusters is enlarged in either row (Fig. 3(c)). This phenomenon occurs when the oscillation frequency of the obstacle is close to twice the vortex shedding frequency and the amplitude is comparable to the healing length. We have studied the amplitude  $a$  and frequency  $\omega$  dependence of the vortex shedding dynamics. The degree of the symmetry breaking of the BvK-like vortex street increases with  $a$  and the periodic street is destroyed for  $a \gtrsim \xi$  (Fig. 3). The  $\omega$  dependence is complicated; the enlargement of the vortex clusters occurs in various ways, as shown in Fig. 4. The sinusoidal motion enhances the symmetry breaking and promotes the transition from vortex dipole generation to BvK-like vortex street generation.

The BvK-like vortex street generation in superfluids is an example of a highly nonlinear phenomenon far from the equilibrium. When some external vibration is applied to such a system and the frequency approaches some resonance, we expect that the system exhibits nontrivial resonant dynamics due to nonlinearity and nonequilibrium.



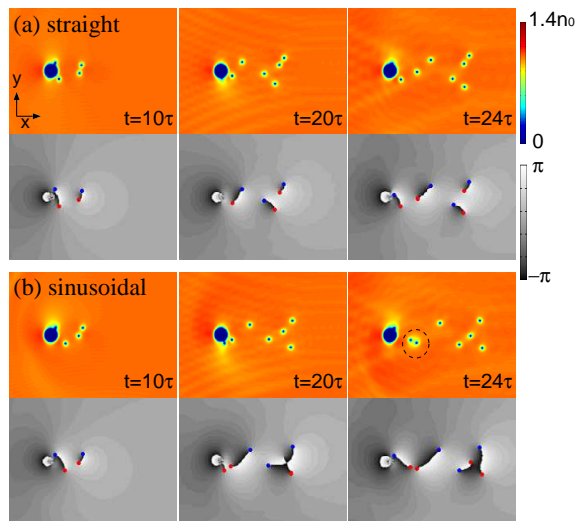


FIG. 5: Snapshots of the density ( $|\psi|^2$ ) and phase ( $\arg \psi$ ) profiles. (a) Without sinusoidal motion. (b) Sinusoidal motion with  $\omega = 0.1\tau^{-1}$  and  $a = 0.32\xi$ . Other parameters are the same as those in Fig. 1(b). The blue and red dots in the phase profiles indicate vortices with clockwise and counterclockwise circulations, respectively. The field of view is  $125\xi \times 95\xi$ .

## Acknowledgments

This work was supported by Grants-in-Aid for Scientific Research (No. 22340116 and No. 23540464) from the Ministry of Education, Culture, Sports, Science and Technology of Japan.

- 
- [1] H. Bénard, Comptes rendus de l'Académie des Sciences, C. R. Acad. Sci. Paris 147 (1908) 839; 147 (1908) 970.
  - [2] T. von Kármán, Über den Mechanismus des Widerstandes, den ein bewegter Körper in einer Flüssigkeit erfährt, Nachr. Ges. Wiss. Göttingen, Math. Phys. Kl. 509 (1911); (1912) 547
  - [3] See, for example, H. Lamb, Hydrodynamics, 6th ed, Dover, New York, 1945.
  - [4] K. Sasaki, N. Suzuki, H. Saito, Bénard-von Kármán vortex street in a Bose-Einstein condensate, Phys. Rev. Lett. 104 (2010) 150404.
  - [5] Hydrodynamic generation of vortex pairs in a Bose-Einstein condensate is reported in T. W. Neely, E. C. Samson, A. S. Bradley, M. J. Davis, B. P. Anderson, Observation of Vortex Dipoles in an Oblate Bose-Einstein Condensate, Phys. Rev. Lett. 104 (2010) 160401.
  - [6] H. Saito, T. Aioi, T. Kadokura, Bénard-von Kármán vortex street in an exciton-polariton superfluid, Phys. Rev. B 86 (2012) 014504.
  - [7] For recent review of exciton-polariton superfluids, see, I. Carusotto, C. Ciuti, Quantum fluids of light, Rev. Mod. Phys. 85 (2013) 299.
  - [8] T. Frisch, Y. Pomeau, S. Rica, Transition to dissipation in a model of superflow, Phys. Rev. Lett. 69 (1992) 1644.
  - [9] B. Jackson, J. F. McCann, C. S. Adams, Vortex Formation in Dilute Inhomogeneous Bose-Einstein Condensates, Phys. Rev. Lett. 80 (1998) 3903.
  - [10] T. Winiecki, J. F. McCann, C. S. Adams, Pressure Drag in Linear and Nonlinear Quantum Fluids, Phys. Rev. Lett. 82 (1999) 5186.
  - [11] C. Nore, C. Huepe, M. E. Brachet, Subcritical Dissipation in Three-Dimensional Superflows, Phys. Rev. Lett. 84 (2000) 2191.
  - [12] J. S. Stieβberger, W. Zwerger, Critical velocity of superfluid flow past large obstacles in Bose-Einstein condensates, Phys. Rev. A 62 (2000) 061601(R).
  - [13] C. Huepe, M. E. Brachet, Scaling laws for vortical nucleation solutions in a model of superflow, Physica D 140 (2000) 126.
  - [14] A. Aftalion, Q. Du, Y. Pomeau, Dissipative Flow and Vortex Shedding in the Painlevé Boundary Layer of a Bose-Einstein Condensate, Phys. Rev. Lett. 91 (2003) 090407.
  - [15] O. M. Griffin, S. E. Ramberg, The vortex street wakes of vibrating cylinders, J. Fluid Mech. 66 (1974) 553.
  - [16] C. H. K. Williamson, A. Roshko, Vortex formation in the wake of an oscillating cylinder, J. Fluids and Structures 2 (1988) 355.
  - [17] W. H. Press, S. A. Teukolsky, W. T. Vetterling, B. P. Flannery, Numerical Recipes, 3rd ed, Sec. 20.7, Cambridge Univ. Press, Cambridge, 2007.
  - [18] T. Aioi, T. Kadokura, T. Kishimoto, and H. Saito, Controlled generation and manipulation of vortex dipoles in a Bose-Einstein condensate, Phys. Rev. X 1 (2011) 021003.
  - [19] Movies showing the dynamics of the density profile are attached to this preprint.
  - [20] G. A. El, A. Gammal, and A. M. Kamchatnov, Oblique Dark Solitons in Supersonic flow of a Bose-Einstein Condensate, Phys. Rev. Lett. 97 (2006) 180405.
  - [21] I. Carusotto, S. X. Hu, L. A. Collins, and A. Smerzi, Bogoliubov-Čerenkov Radiation in a Bose-Einstein Condensate Flowing against an Obstacle, Phys. Rev. Lett. 97 (2006) 260403.